Journal of Geological Remote Sensing 2023 1(1);56-72

Graduate University of Advanced Technology

Journal of Geological Remote Sensing

Journal homepage: https:// jgrs.kgut.ac.ir

Iranian Geological Remote Sensing Society

Assessment of Classification Mapping for the Purposes of Geologic Mapping and Practical Utility in the Field Geology Workflow: An Example from Southern Death Valley

Zachariah D. Fleming*

Assistant Professor – Stephen F Austin State University

Article Info

Keywords:
ASTER
Remote Sensing
Classification
Death Valley
Geologic Mapping

Abstract

This study presents an example of multi-spectral classification mapping, in the Ibex Hills, CA, USA, which was used to support field endeavors, the results of which were then compared to recent geologic mapping in order to assess the classification results. To do this a combination of ENVI and QGIS softwares, using bands 1-9 of Advanced Spaceborne Thermal Emission and Reflection Radiometer (ASTER) multi-spectral data, were used to create supervised classification maps. The inputs into the supervised classifications were combinations of Principal Component Analysis (PCA) of the ASTER bands and ASTER band ratios. The results herein showed that utilizing a combination of both PCA and band ratios for classification resulted in the most accurate results when compared to the training data. Two different classification algorithms were compared, Parallelepiped and Maximum Likelihood (ML), which both performed at a similar overall accuracy, ~54%, but varied in effectiveness with different lithologies with the Parallelepiped excelling at gneiss and mafic intrusive units, at ~85%+ accuracy, and Maximum Likelihood excelling at identifying shales, at ~72% accuracy. While issues remain with classifying certain lithologies the classification maps provided a useful, albeit coarse, tool for field work. Although the methodologies of this study are not original, the heterogeneity inherent in geologic field sites can result in a variety of spectral signatures for similar lithologies, thus making case-studies of specific regions an important tool for future work in those areas.

*Corresponding author.
Email: zachariah.fleming@sfasu.edu

https://doi.org/10.48306/jgrs.2024.413843.1005
Received 29 Aug. 2023; Received in revised form 15 Mar. 2024; Accepted 28 Apr. 2024
Available online 22 June 2024

1. Introduction

Classification mapping using multi-spectral data has long been shown to identify lithologies for the purposes of geologic mapping and, in some cases, shown to obtain a high degree of accuracy when compared to ground truthing (Aboelkhair et al., 2020; Ali-Bik et al., 2018; Bertoldi et al., 2011; Siegal & Abrams, 1976). In terms of conducting geologic field mapping, it has been recognized that classification maps can provide valuable insight into the general map pattern of an area, potential "problem areas" to focus on, and potentially help to guide contacts drawn in areas that are difficult to physically map (Bertoldi et al., 2011; Quick & Hogan, 2022). This study utilized 9 bands of ASTER multi-spectral data which ranged from the Very Near Infrared (VNIR) (3 bands) to Short-wave Infrared (SWIR) spectrum (6 Bands), acquired on November, 8th 2015, in order to create a classification map of the northern Ibex Hills in Death Valley, CA (Table 1). Ultimately the goal of this study was to assess how supervised classification maps can be integrated into the geologic mapping workflow of the southern Death Valley area, similar to work that has recently been done in other field locales (Quick & Hogan, 2022). Additionally, there is still the need for case studies identifying lithologic units across specific sites since lithologic characteristics commonly change depending upon the study area due to variations in weathering, exposure, and unit specific characteristics (Gomez et al., 2005; Jakob et al., 2015).

ASTER Band	Wavelength (μm)	Spatial Resolution (m)
1	0.52-0.6	15
2	0.63-0.69	15
3	0.76-0.86	15
4	1.6-1.7	15
5	2.145-2.185	30
6	2.185-2.225	30
7	2.235-2.285	30
8	2.295-2.365	30
9	2.360-2.430	30

Table 1. Wavelength and spatial resolution for each of the nine ASTER bands used in this study.

Two programs were used for image processing, the first was ENVI and the second was QGIS along with the Semi-Automatic Classification Plugin (Congedo, 2021). In either case all the techniques utilized in this study are functions readily available in the programs and/or plugins. While the techniques presented herein are not new, the band ratios themselves, including the band math involving principal component analysis (PCA), were empirically determined for the study area. In order to assess the accuracy of the techniques the results were compared to lithologic field mapping of the area (Fleming et al., 2021). The field mapping itself was actually aided by the

classification maps of this study, as they provided insight into the broader map pattern and areas of potential interest. Thus, this is a prime example of how remote sensing and field geology can work in tandem to produce a geologic map.

The study area for this paper is the Ibex Hills, CA, located in a region of low vegetation which makes the application of remote sensing techniques ideal and also provides plentiful access to ground truthing (Figure 1). Although during the process of mapping this area, beyond this project, the use of simple ortho-imagery was effective at times there are certain units in the Ibex Hills which are difficult to discern by imagery alone. The use of the techniques of this study were therefore an effective way to improve the accuracy of the geologic map (Fleming et al., 2021) and provided initial constraints on where to focus field efforts.

The primary methods used in this project were band ratios, PCA, Parallelepiped classification, and Maximum Likelihood (ML) classification. Combinations of the processed data alongside the unprocessed (beyond atmospheric correction) ASTER data were used in the classifications in order to evaluate the best way to identify rock units in the Ibex Hills. The accuracy of these combinations was then assessed by the creation of a confusion matrix which reveals the percentage of successfully classified pixels compared to those of a known case, in this study the mapping of Fleming et al. (2021) was the known case.

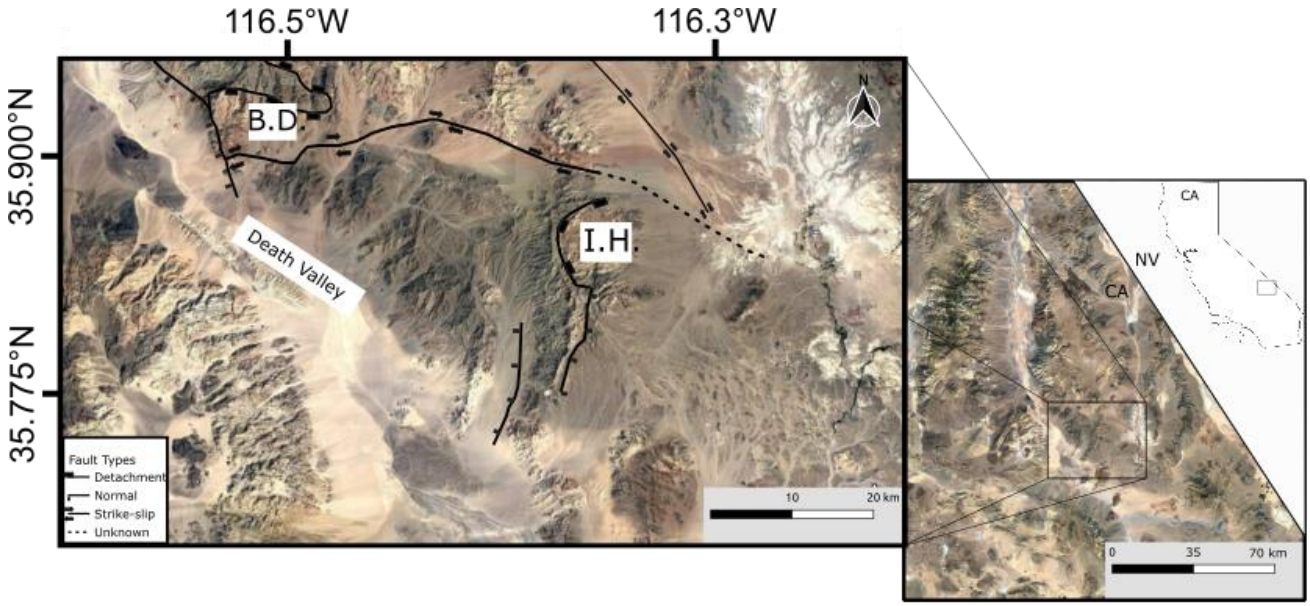

Figure 1. Map showing the general locality of the Ibex Hills (I.H.) along with the Black Mountain Detachment fault (B.D.) and simplified traces of other faults in the area. Box on the right shows the Nevada, USA (NV) and California, USA (CA) border for context. Note that this figure portrays the Ibex Hills as containing a portion of the Black Mountain Detachment Fault. Latitude and longitude shown in WGS84 Web Mercator.

2. Study Area

The Ibex Hills are located in southeastern California, USA and lie in a critical position within the Death Valley extensional terrane (Figure 1), a long-studied area for the purposes of understanding continental extension and transtension systems (e.g., Burchfiel & Stewart, 1966; Pavlis et al., 2014; Snow & Wernicke, 1989, 2000; Wright et al., 1976). Despite this amount of study there is still debate on the nature of Neogene extension throughout the area, with evidence for accommodation along both regional detachments and more localized normal faulting (Miller & Pavlis, 2005). The Ibex Hills have been previously cited as containing the up-dip portion of the Black Mountain Detachment, a critical structure in the aforementioned debate (Figure 1) (Holm & Dokka, 1993; Holm & Wernicke, 1990, 1990; Topping, 1993). However, more recent mapping has pushed back on this claim, illustrating that the Ibex Hills is an important area for understanding the Neogene deformation of southern Death Valley at large. Thus, techniques that enhance mapping both pre- and post-field, such as those in this study, remain useful for future work in an area that strongly relies on detailed geologic mapping.

The exposed bedrock of the area are as follows; 1.4 Ga basement gneiss, the Neoproterozoic Pahrump Group which includes the Crystal Springs Formation, Horse Thief Springs Formation, and the Becks Spring Dolomite, and the overlying Noonday Formation, Johnnie Formation, Zabriski Quartzite, and Wood Canyon Formation (Figure 2) (Fleming et al., 2021). The Pahrump Group and overlying units record the evolution of the southwestern edge of Laurentia and associated miogeocline deposits, with the Pahrump Group having been deposited in a regional extensional basin, first described by Wright et. al. (1976) as the Amargosa Aulacogen. Within these units there are many overlaps of lithology, therefore, this work will focus on delineating dolomite, shale, gabbro, quartzite, and gneiss, which are exposed throughout the Ibex Hills (Figures 2 and 3).

While there has been geologic mapping work done in the Ibex Hills and surrounding southern Death Valley region, none has been in the context of remote sensing. Furthermore, despite the relationship of the Ibex Hills to major structures nearby there had been few published geologic maps, one of which is the Wright & Troxel, (1968) map of the central Ibex Hills where the major detachment in the range is mapped as a thrust fault, until the recent mapping by Fleming et al. (2021). Other topical studies have also examined the stratigraphy (Corsetti & Kaufman, 2003); Workman et al.'s (Workman et al., 2002) USGS 1:250k compilation included updated mapping from unpublished work by L. Wright and B. Troxel. This dearth of published mapping provides a unique opportunity to test the ability of remote sensing techniques to be used in the region which, in turn, can also be of use for future interpretation of areas with the same exposed rock units.

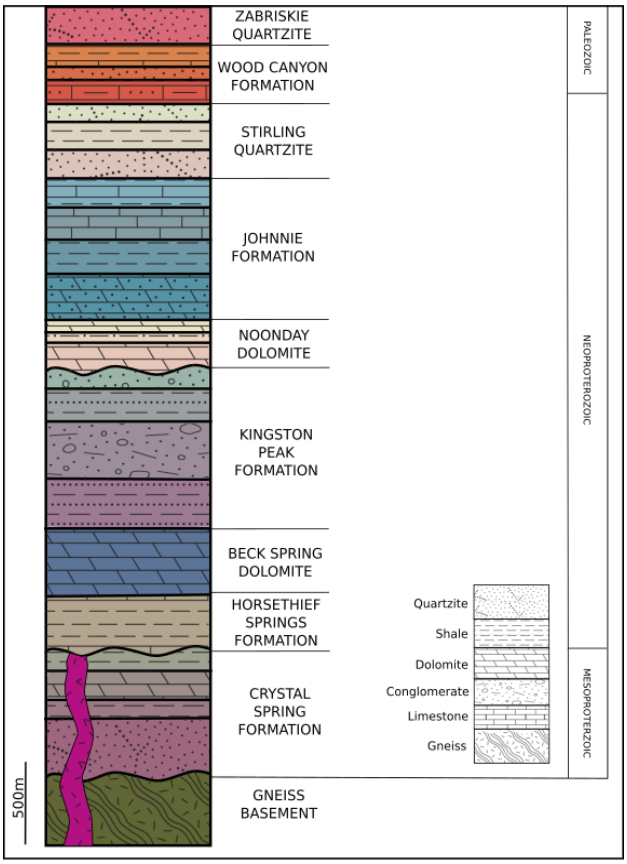

Figure 2. Stratigraphic column of the bedrock units in the study area, formations are sub-divided by thick black lines. Patterns in the lower right show the lithologies used in the column. Note that the columns show mixed patterns in some units (e.g. Wood Canyon) which simply indicate interbedded unit lithologies.

3. Methods

Data was acquired via the NASA Reverb site (http://reverb.echo.nasa.gov/reverb/) as Level 2 surface reflectance. This contained an ASTER scene containing bands in the Visible Near Infrared (VNIR) and Short-wave Infrared (SWIR). Since ASTER VNIR data is collected at 15m pixel resolution and the SWIR was collected at 30m pixel resolution the image data was resized so it could be used as a cohesive data set. Using the Resize Data (Spatial/Spectral) functionality within ENVI the VNIR data was resized from 15m pixel resolution to 30m. The choice was made to resize the 15m VNIR data because there are more bands in the SWIR, as well as to avoid creating higher resolution data product from the lower resolution data source.

The layers, after being resized, were then clipped to the general study area (Figure 3), using a Region of Interest (ROI) to clip, due to the large size of the originally ASTER scene. The methodologies used to further analyze the ASTER data in the new clipped area are described in the following sections. The data associated with these methods, a collection of header and image files of ASTER data, for use in ENVI software, is freely available with the data repository Zenodo (zenodo.org) and the direct link to the data is provided in the Data Availability Statement, following the conclusions section.

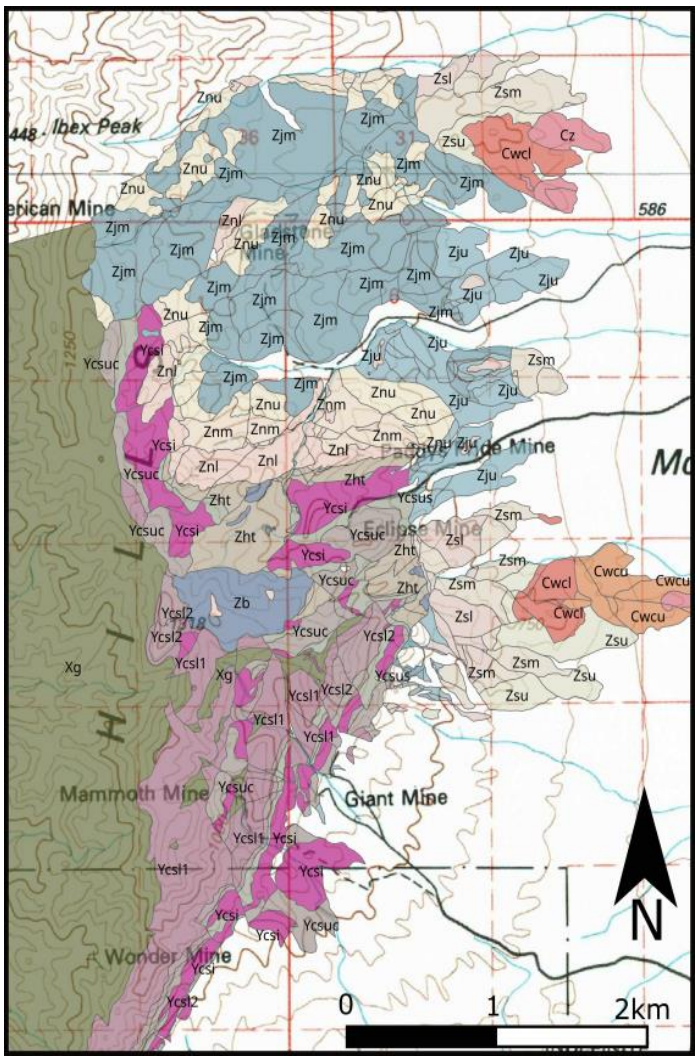

Figure 3. Simplified geologic map of the northern Ibex Hills, unit labels follow those of the stratigraphic column of Figure 2. Note that this map shows much more diversity than the classification maps as the classifications are aimed at lithology. The lithologies of the various units are also shown in Figure 2 by the patterns and legend. Adapted from Fleming et al. (2021).

3.1 Band Ratios

The first set of data products created for use in the classification of the Ibex Hills site were band ratios using the VNIR and SWIR bands of the ASTER data. To do this spectrum of the different lithologies were compared manually in order to recognize differences. This was done by analyzing the spectral profiles of pixels across areas of clear lithologic changes (Figure 4). Based on these observations, the ratios used were band1/band2, band5/band6, and band6/band7. Band1/band2 was based on upon the virtually flat to negative slope from band 1 to band 2, representing an absorption feature near band 2 for the intrusive gabbro and basement rock, compared to the steep positive change seen in the Noonday Dolomite and other units. Band5/band6 was based upon the steep absorption seen at band 5 in all studied rock units except for the Lower Crystal Springs/quartzite units and

the basement gneiss. Finally, the band6/band7 ratio was chosen due to absorption at band 6, seen in only the lower Crystal Spring quartzite and basement gneiss. These ratios were created via the Band Ratio function available in ENVI and the resulting band ratios were then stacked into one layer.

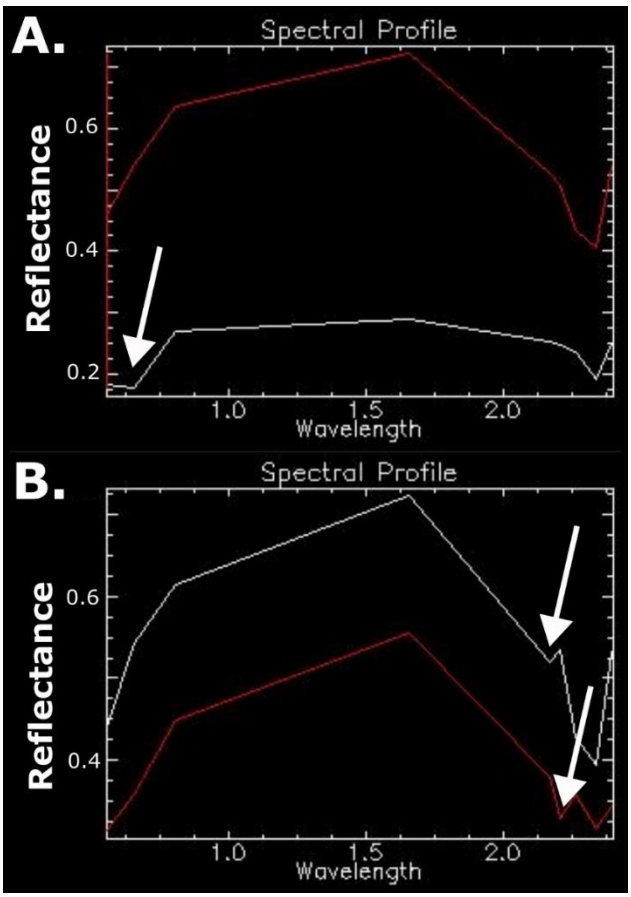

Figure 4. Example spectral profiles from the study area which were used to define band ratios. A. Lower profile shows absorption at ASTER band 2, indicated by the arrow, for the basement gneiss. The upper profile shows the Noonday dolomite for comparison. B. Upper profile shows an example of the absorption at ASTER band 5 seen in most units, in this example an area of the Horse Thief Springs Formation, but less so in the lower Crystal Springs quartzite, shown in the lower profile. The lower profile exhibits an absorption at ASTER band 6 seen in the lower Crystal Springs and basement gneiss.

3.2 Principal Component Analysis

PCA is a widely used statistical technique in which the coordinate system of a set of variables, ASTER band images in the case of this study, is transformed such that the new axes correspond to the maximum variance across the data (Demšar et al., 2013; Greenacre et al., 2022). The results of PCA have been used extensively in remote sensing and classification mapping to delineate lithologic changes (Demšar et al., 2013; Jakob et al., 2015; Quick & Hogan, 2022). PCA was performed on the original data set in order to create a new set of bands which would optimize the contrast between units. Each band in this analysis represents an axis in the 9-dimensional point cloud of ASTER data, and thus, they contain values based upon the actual variability within the spectrum from each band.

3.3 Supervised Classification

Two supervised classification algorithms were used in this study, the first of which was the parallelepiped classification in ENVI. Parallelepiped classification is a decision rule-based classification method which relies on the mean value and standard deviation of a selected training class, the ROIs created in ENVI in this case, to form the decision boundaries (Sathya & Deepa, 2017). If a pixel falls within the boundaries of this box it is considered to be part of that class. The advantage of the parallelepiped algorithm is computationally efficient; however, it commonly results in unclassified pixels (Sathya & Deepa, 2017). The second classification algorithm used was ML which instead calculates a probability for whether a given pixel belongs to a training class based on a probability density function for that class (Sathya & Deepa, 2017). Maximum likelihood algorithms tend to provide strong separation of classes, and thereby limit unclassified pixels, however, they do require more well-defined training classes (Sathya & Deepa, 2017).

Considering that a major goal of this study was to create an accurate classification map of the study area, it was decided to first create a map using only the original unprocessed, apart from resizing, correction, etc., ASTER data. To do this a set of ROIs were created, which act as training classes for the classification algorithm, representing the units exposed in the area. Specifically, ROIs were created for the basement gneiss, the lower Crystal Springs quartzite, the intrusive gabbro, the Noonday dolomite, and the Horse Thief Springs shales. Other ROIs for the area were neglected due to repetitions of lithology (Figure 2). Therefore, the Noonday ROI is meant to represent dolomite in general, which is found in upper Crystal Springs and Beck Springs as well, the Horse Thief ROI represents shales which are also found in the Middle Noonday Formation, and the lower Crystal Springs represents quartzite. These ROIs were saved and used for each classification performed in this study. The stacked raw data was selected as the input file within ENVI and the saved ROIs were used for the different classes. A mask was also created in order to ignore the basin fill surrounding the range that will not classify well with bedrock endmembers. The result was a classification based only upon the original reflection data (Figure 5A). The initial choice of the parallelepiped algorithm for classification was simply based on the qualitative observation, through earlier attempts during this work, that this algorithm created the most acceptable maps compared to the ongoing field mapping in the study area. However, in order to better estimate the utility of remote sensing in this area, the results of the most accurate parallelepiped classification map were compared to a classification map using maximum likelihood (Figure 6).

Using the same workflow described above, for the raw data classification, maps were created for both the band ratio and principal component layers using their respective bands (Figure 5B and 5C). A combination layer of all the band ratios and PCA's was also created via layer stacking (Figure 5D). In addition, a combination of the band ratios and PC3 was created in an attempt to heighten the contrast seen between Lower Crystal Springs and the basement rock, which was lacking in just the band ratio classification but evident in the PC3 band (Figure 5). Inclusion of the lower PC bands led to a decrease in the accuracy the accuracy, presumably due to the noise inherent in the lower PC bands.

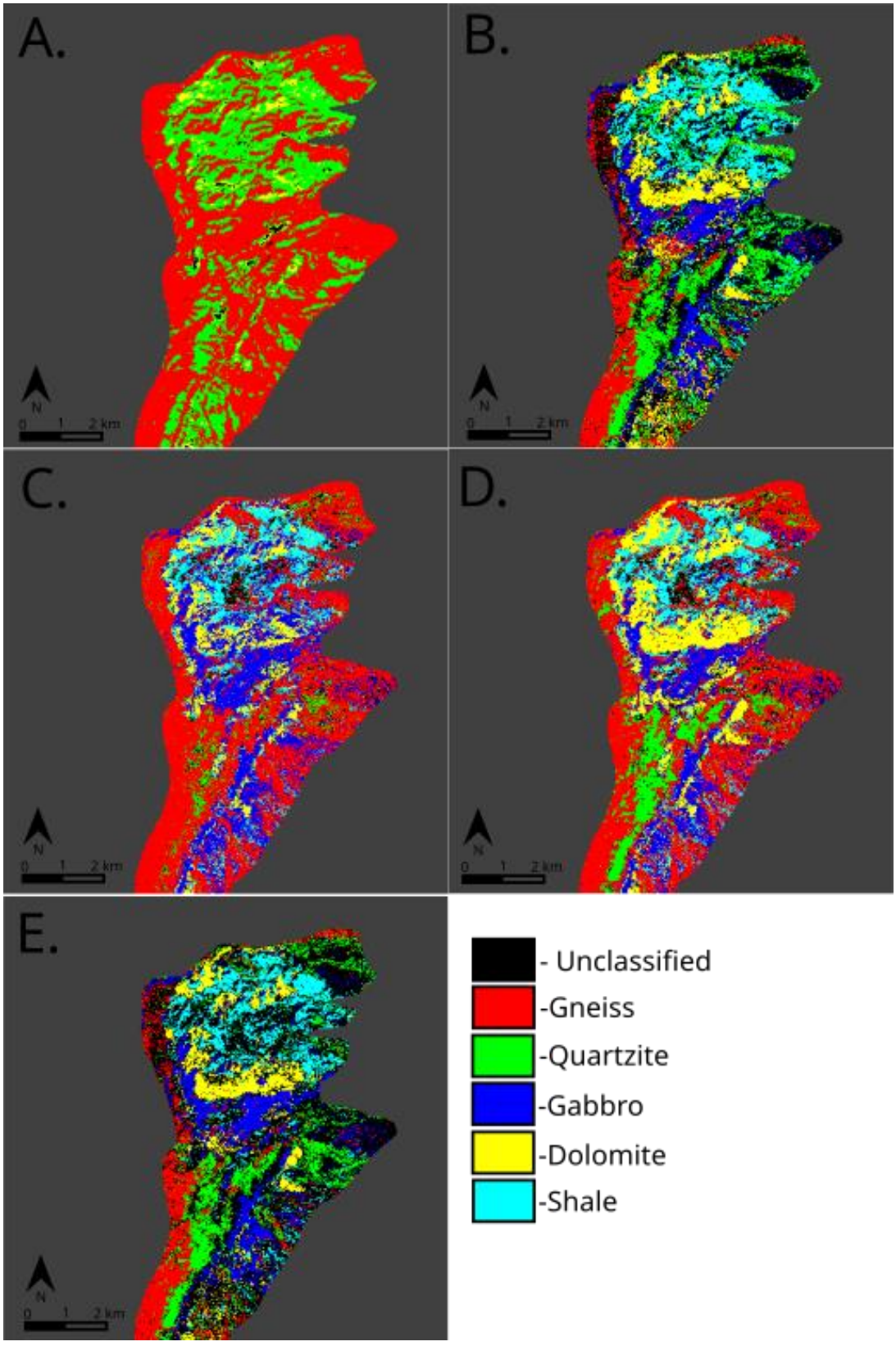

Figure 5. Classification maps produced by this study using the parallel-piped algorithm. A. Classification using raw ASTER data B. Classification using Band Ratios C. Classification using PCA only D. Classification using Band Ratios and PC3 E. Classification using all Band Ratios and PC bands.

Using the same ROI areas as the parallelepiped classification done in ENVI, a ML classification was done in the software QGIS using the Semi-Automatic Classification Plugin (Congedo, 2021). This classification was done only for the dataset of band ratios and the PC3 band because this combination yielded the best accuracy when compared to the ROIs, which will be discussed in the following section, and, therefore, is the preferred dataset for classification in the area (Figure 6).

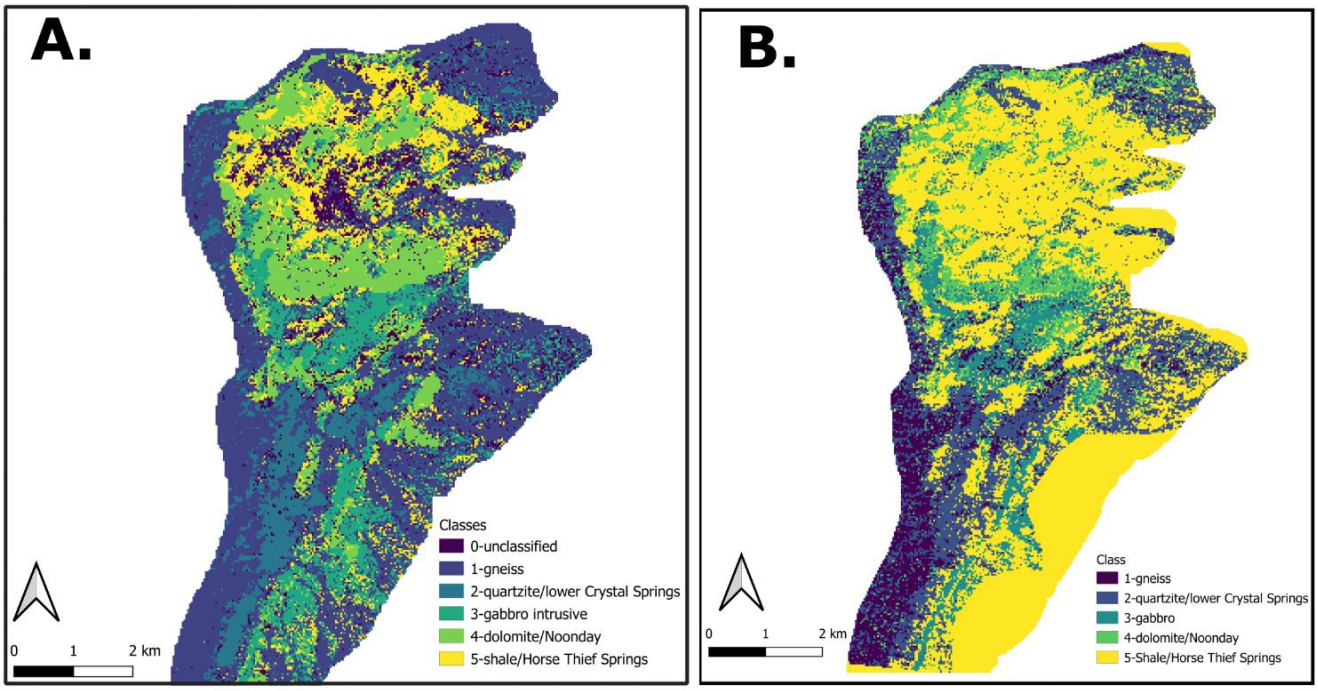

Figure 6. Classification results of the parallelepiped algorithm (A) and the maximum likelihood algorithm (B). In both cases the inputs were the same training ROIs using the band ratios determined from this study and the PC3 band.

3.4 Accuracy Assessment

In order to evaluate the accuracy of each classification map a confusion matrix was calculated for each map using the training ROIs, which were themselves based on known areas from geologic mapping (Figure 3). The results of a confusion matrix contain the percentage of correctly identified pixels in each ROI, as well as unclassified pixels and those incorrectly classified. The results of the confusion matrix calculations are shown in Table 2. Two additional confusion matrices were then calculated for the map area as whole, using the mapping of Fleming et al. (2021) as the reference input, for the classification maps using the combination of band ratios and PC3, for both parallelepiped and maximum likelihood classification (Table 3 and 4). In order utilize the mapping of Fleming et al. (2021), the Dissolve tool was used in QGIS to dissolve all polygons of the same lithology together. A new field was then added to the dissolved units which corresponded to the training inputs and the polygons were then converted using the Rasterize tool in QGIS.

Inputs Used	Overall Accuracy	Basement	Lower Crystal Spring	Intrusive	Noonday/Dolomite	Shale
ASTER Reflectance Bands 1-9	54.03%	92.75	80.46	0	28.28	0
Band Ratios: b1/b2, b5/b6, b6/b7	75.92%	99.31	35.06	89.8	68.28	29.03
Principal Component Analysis	74.04%	80.31	87.36	86.94	81.38	19.35
Band Ratios and PC3	82.39%	86.87	91.95	89.39	97.93	38.17
Combined Band Ratios and PCA	74.12%	80.14	82.76	91.43	80.69	19.35

Table 2. Columns show percent accuracy for each classification, when compared to the ROI, based on their inputs.

ERROR MATRIX [pixel count]						
Classification Result	0	1	2	3	4	5
0	0	39	333	7	681	2198
1	0	5234	1909	114	1305	3294
2	0	657	3445	0	333	249
3	0	45	38	825	1596	1519
4	0	11	114	23	5667	1702
5	0	12	93	7	803	5420
Total Pixels	0	5998	5932	976	10385	14382
PA (%)		87.26	58.07	84.52	54.56	37.68
UA (%)		44.14	73.54	20.50	75.38	85.55

Table 3. Accuracy results of the parallelepiped classification map, using the inputs of the band ratios and PC3. The rows represent the classification results and the columns represent the number of pixels of each reference class (i.e., the geologic map) classified as such. The lowest two rows display the Producer's Accuracy (PA) and the User's Accuracy (UA) for each class. The classes are as follows: 1 – gneiss, 2 – quartzite/lower Crystal Springs, 3 – gabbro, 4 – dolomite/Noonday, and 5 – shale/Horse Thief Springs.

ERROR MATRIX [pixel count]					
Classification Result	1	2	3	4	5
1	3070	1132	58	454	187
2	2164	3452	62	1160	1424
3	194	129	669	1920	726
4	415	237	147	2743	1726
5	155	982	40	4108	10319
Total Pixels	5998	5932	976	10385	14382
PA (%)	51.1837	58.1929	68.5451	26.4131	71.7494
UA (%)	62.6403	41.7817	18.3892	52.0691	66.1305

Table 4. Accuracy results of the maximum likelihood classification map, using the inputs of the band ratios and PC3. The rows represent the classification results and the columns represent the number of pixels of each reference class (i.e., the geologic map) classified as such. The lowest two rows display the Producer's Accuracy (PA) and the User's Accuracy (UA) for each class. The classes are as follows: 1 – gneiss, 2 – quartzite/lower Crystal Springs, 3 – gabbro, 4 – dolomite/Noonday, and 5 – shale/Horse Thief Springs.

4. Results and Discussion

4.1 Accuracy of Classification Mapping

The goals of this project were to assess the accuracy of classification maps derived from ASTER imagery in the area of the Ibex Hills and, also, to assess the utility of said classification maps as tools for boots-on-the-ground geologic mapping. When looking at the accuracy of the classification maps as compared to the training ROIs, they varied based on their input bands, which is to be expected, and, in order to find the best result, different combinations of bands, band ratios, and principal components were analyzed. The unprocessed ASTER bands gave the least accurate results by far, with an overall accuracy of 54.03% (Table 2). The biggest problem with this classification was that it grossly overestimated the amount of basement gneiss present in the area (Figure 5). The classification built with the band ratio's fared much better with an overall accuracy of 75.92% (Table 2). The primary issue with this result was that much of the clastic portion of the lower Crystal Springs was identified as the basement rock (Figures 5). This was not surprising as none of the band ratios gave a strong contrast between the two lithologies. Also, in the band ratio classification, much of the Horse Thief/Shale ROI was classified as a mix of other units (Table 2). This, however, was expected to be a problem due to the variable spectrum seen in those units and the fact that multiple units contained shale members and so portions of them were likely to be lumped into this class (Figure 2). The classification of PC bands had a similar accuracy of 74.04%, however, there were improvements seen when compared to the band ratios (Table 2). While the accuracy of the basement rock

classification dropped, the lower Crystal Spring and Noonday/Dolomite accuracy increased significantly. Although the accuracy for the shale classification decreased there were less pixels which were wrongly classified and more unclassified pixels; a preferable outcome when considering using the results for geologic mapping. The combination of band ratios with PC3 gave the highest overall accuracy when compared to the training ROIs at 82.39% (Table 2). Again, some of the basement was classified as lower Crystal Springs, however, it was mostly correct. The shale was the biggest problem with many pixels being wrongly classified but every other class of lithology had strong results (Table 2). The combination of all the band ratios and PC bands together gave an overall accuracy of 74.12%, however, most of the inaccuracy came in the way of unclassified pixels and not incorrectly classified pixels. This is especially true with the shale class which was >70% unclassified (Table 2).

Based on the initial accuracy assessment the combination of band ratios and the PC3 band is the preferred classification input for this area (Table 2). In order to better assess how useful these data might be, the classification using band ratios and the PC3 band was also run using the maximum likelihood algorithm. The results of this, along with the classification using the parallelepiped algorithm, were then compared to the mapping of Fleming et al. (2021). The overall accuracy of the two algorithms was similar, with the parallelepiped classification performing at 54.7% and the maximum likelihood classification performing at 53.8% (Table 3 and 4). However, when considering individual classes, the two algorithms performed quite differently. In the case of the parallelepiped classification map, and looking specifically at the Producer's Accuracy (PA), the classes representing the basement gneiss and the intrusive gabbro were most accurate, performing at 87.2% and 84.5%, respectively. The maximum likelihood classification on the other hand, and again looking at PA, performed best with the classes representing the gabbro intrusive and the shales, performing at 68.5% and 71.7%, respectively. It is worth noting that the shale class was the least accurate class of the parallelepiped classification, suggesting a combination of classification algorithms may work best in this area.

It is interesting to note that in no case was the Beck Spring Dolomite successfully classified. It was expected that it would be classified within the Noonday/dolomite class due to similar lithology, however, it was not under any of the classification scenarios. This was noted in earlier version of the classification maps and, when field work in the area was done, it was recognized that the Beck Spring Dolomite deposits in the Ibex Hills are highly brecciated and mostly in fault contact with other units (Fleming et al., 2021). This textural difference may have significantly influenced the spectral signature seen in the Beck Spring Dolomite and ultimately made it a difficult unit to classify. Therefore, future work would likely need to create a separate class for brecciated dolomites. This apparent incongruity of the Beck Spring and Noonday dolomites is a prime example of the value of case-studies like this one; these units are the same rock type yet textural aspects (i.e., brecciation) which influence their classification.

4.2 Utility for Geologic Field Mapping

The results of this study suggest that while the overall accuracy of classification mapping using ASTER data may be limited when compared to detailed geologic mapping, there is no doubt utility in conducting remote sensing analysis before, and after, conducting field work. This is something that has been recognized previously

in other locales (Quick & Hogan, 2022). When planning for field mapping in the study area the author analyzed the results of the classification maps in order to assess potential problem areas in which to focus field time. In the study area the most apparent problem areas were those that show clearly repeated rock units, a map pattern which inherently requires geologic structure and, ultimately, those turned out to be highly faulted areas (Figure 7). Additionally, with the classification methods of this study, future work can potentially make use of ASTER data to classify and map out similar lithologies throughout the area and, based on this works accuracy assessment, have an understanding of how reliable those maps may be.

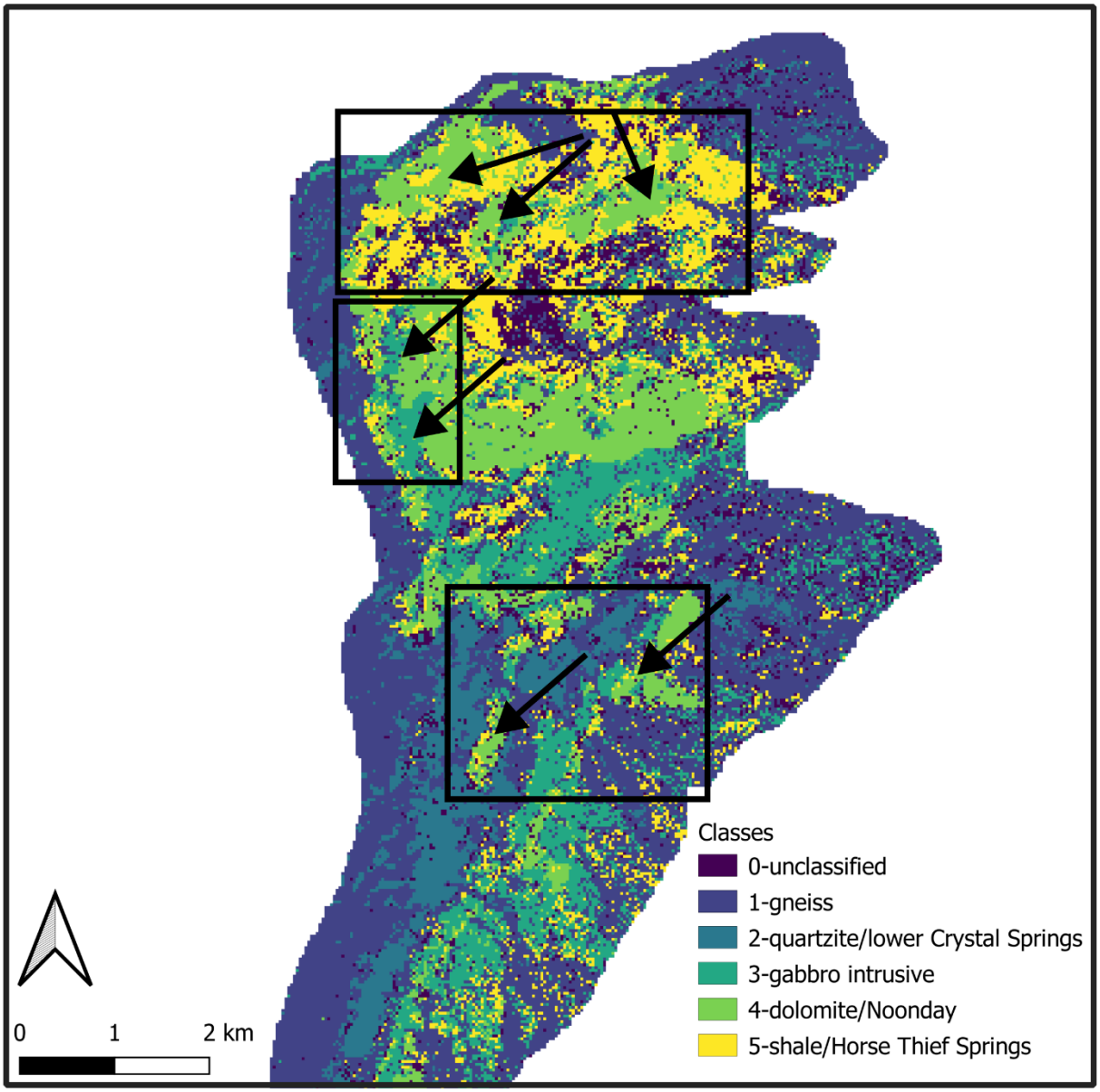

Figure 7. Classification map resulting from the parallelepiped algorithm with geologic "problem areas" in boxes. These are areas which influenced decisions on how to utilize time in the field. Arrows indicate repeated lithology within those boxed areas, suggesting geologic structure.

5.Conclusions

The use of ASTER multi-spectral data has the potential to enhance the geologic mapping process, especially in well exposed regions. Recent mapping (Fleming et al., 2021) in the Ibex Hills, CA provides an ideal opportunity to test remote sensing methods in this region (Figure 3). The combination of band ratios with PC3 gave the most overall accuracy when compared to using just band ratios, just PC bands, or a combination of all processed bands (Table 2). Using that preferred set of data classification maps were created using both parallelepiped and maximum likelihood algorithms (Figure 7). When compared to the recent mapping of Fleming et al. (2021), both algorithms were lacking in their overall accuracy, registering at just over 50% accuracy. However, both were able to classify the gabbro unit in the study area well and the parallelepiped classification performed well in classifying the gneiss unit, whereas the maximum likelihood classification performed well in classifying the shale units (Table 3 and 4). In terms of utility for the geologic mapping process, the classification maps revealed areas of potential geologic structures and, therefore, informed the mapping efforts in the Ibex Hills and suggest it is a useful, if limited, tool for geologic mapping routines (Figure 7).

6.Data Availability Statement

The data the support the findings of this study can be found in the data repository Zenodo with the following DOI: 10.5281/zenodo.4308973.

7.Acknowledgements

The author would like to thank the Department of Earth Sciences and Geologic Resources at Stephen F Austin State University for the access to computers and software needed for this study. Additionally, a thank you to the reviewers of this article which resulted in significant improvements to the writing and methodology.

8.References

Aboelkhair, H., Abdelhalim, A., Hamimi, Z., & Al-Gabali, M. (2020). Reliability of using ASTER data in lithologic mapping and alteration mineral detection of the basement complex of West Berenice, Southeastern Desert, Egypt. *Arabian Journal of Geosciences*, *13*(7), 287. https://doi.org/10.1007/s12517-020-5227-x

Ali-Bik, M. W., Hassan, S. M., Abou El Maaty, M. A., Abd El Rahim, S. H., Abayazeed, S. D., & Wahab, W. A. (2018). The late Neoproterozoic Pan-African low-grade metamorphic ophiolitic and island-arc assemblages at Gebel Zabara area, Central Eastern Desert, Egypt: Petrogenesis and remote sensing - Based geologic mapping. *Journal of African Earth Sciences*, *144*, 17–40. https://doi.org/10.1016/j.jafrearsci.2018.04.001

Bertoldi, L., Massironi, M., Visonà, D., Carosi, R., Montomoli, C., Gubert, F., Naletto, G., & Pelizzo, M. G. (2011). Mapping the Buraburi granite in the Himalaya of Western Nepal: Remote sensing analysis in a collisional belt with vegetation cover and extreme variation of topography. *Remote Sensing of Environment*, *115*(5), 1129–1144. https://doi.org/10.1016/j.rse.2010.12.016

Burchfiel, B. C., & Stewart, J. H. (1966). "Pull-Apart" Origin of the Central Segment of Death Valley, California. *Geological Society of America Bulletin*, *77*(4), 439–442. https://doi.org/10.1130/0016-7606(1966)77[439:POOTCS]2.0.CO;2

Congedo, L. (2021). Semi-Automatic Classification Plugin: A Python tool for the download and processing of remote sensing images in QGIS. *Journal of Open Source Software*, *6*(64), 3172. https://doi.org/10.21105/joss.03172

Corsetti, F. A., & Kaufman, A. J. (2003). Stratigraphic investigations of carbon isotope anomalies and Neoproterozoic ice ages in Death Valley, California. *Geological Society of America Bulletin*, *115*(8), 916–932. https://doi.org/10.1130/B25066.1

Demšar, U., Harris, P., Brunsdon, C., Fotheringham, A. S., & McLoone, S. (2013). Principal Component Analysis on Spatial Data: An Overview. *Annals of the Association of American Geographers*, *103*(1), 106–128. https://doi.org/10.1080/00045608.2012.689236

Fleming, Z. D., & Pavlis, T. L. (2015). Multiple phases of low-angle normal faulting from the Precambrian to the Neogene in the Ibex Hills and Saratoga Hills, CA. *Abstracts with Programs - Geological Society of America*, *47*(7), 149.

Fleming, Z. D., & Pavlis, T. L. (2018). Structural analysis of the ibex hills, Ca: Evidence for multiple phases of Mesozoic shortening and transtensional related folding, faulting, and extension. *Abstracts with Programs - Geological Society of America*, *50*(5), Abstract no. 18-3.

Gomez, C., Delacourt, C., Allemand, P., Ledru, P., & Wackerle, R. (2005). Using ASTER remote sensing data set for geological mapping, in Namibia. *Physics and Chemistry of the Earth, Parts A/B/C*, *30*(1–3), 97–108. https://doi.org/10.1016/j.pce.2004.08.042

Greenacre, M., Groenen, P. J. F., Hastie, T., D'Enza, A. I., Markos, A., & Tuzhilina, E. (2022). Principal component analysis. *Nature Reviews Methods Primers*, *2*(1), Article 1. https://doi.org/10.1038/s43586-022-00184-w

Holm, D. K., & Dokka, R. K. (1993). Interpretation and tectonic implications of cooling histories: An example from the Black Mountains, Death Valley extended terrane, California. *Earth and Planetary Science Letters*, *116*(1–4), 63–80. https://doi.org/10.1016/0012-821X(93)90045-B

Holm, D. K., & Wernicke, B. (1990). Black Mountains crustal section, Death Valley extended terrain, California. *Geology*, *18*(6), 520–523. https://doi.org/10.1130/0091-7613(1990)018<0520:BMCSDV>2.3.CO;2

Jakob, S., Bühler, B., Gloaguen, R., Breitkreuz, C., Eliwa, H. A., & El Gameel, K. (2015). Remote sensing based improvement of the geological map of the Neoproterozoic Ras Gharib segment in the Eastern Desert (NE–Egypt) using texture features. *Journal of African Earth Sciences*, *111*, 138–147. https://doi.org/10.1016/j.jafrearsci.2015.07.024

Miller, M. B., & Pavlis, T. L. (2005). The Black Mountains turtlebacks: Rosetta stones of Death Valley tectonics. *Earth-Science Reviews*, *73*(1–4), 115–138. https://doi.org/10.1016/j.earscirev.2005.04.007

Pavlis, T. L., Rutkofske, J., Guerrero, F., & Serpa, L. F. (2014). Structural overprinting of Mesozoic thrust systems in eastern California and its importance to reconstruction of Neogene extension in the southern Basin and Range. *Geosphere*, *10*(4), 732–756. https://doi.org/10.1130/GES00993.1

Petterson, R., Prave, A. R., Wernicke, B. P., & Fallick, A. E. (2011). The Neoproterozoic Noonday Formation, Death Valley region, California. *Geological Society of America Bulletin*, B30281.1. https://doi.org/10.1130/B30281.1

Quick, J. D., & Hogan, J. P. (2022). Practical remote sensing data analysis for efficient geological field mapping: An example from the southwest portion of the Three Peaks 7.5′ quadrangle, southwest Utah. *Rocky Mountain Geology*, *57*(2), 117–135. https://doi.org/10.24872/rmgjournal.57.2.117

Sathya, P., & Deepa, V. B. (2017). Analysis of Supervised Image Classification Method for Satellite Images. *International Journal of Computer Science Research*, *5*(2), 16–19.

Siegal, B. S., & Abrams, M. J. (1976). Geologic mapping using LANDSAT data. *Photogrammetric Engineering and Remote Sensing*, *42*. https://ntrs.nasa.gov/citations/19760042469

Snow, J. K., & Wernicke, B. (1989). Uniqueness of geological correlations: An example from the Death Valley extended terrain. *Geological Society of America Bulletin*, *101*(11), 1351–1362. https://doi.org/10.1130/0016-7606(1989)101<1351:UOGCAE>2.3.CO;2

Snow, J. K., & Wernicke, B. P. (2000). Cenozoic tectonism in the central Basin and Range; magnitude, rate, and distribution of upper crustal strain. *American Journal of Science*, *300*(9), 659–719. https://doi.org/10.2475/ajs.300.9.659

Topping, D. J. (1993). Paleogeographic reconstruction of the Death Valley extended region: Evidence from Miocene large rock-avalanche deposits in the Amargosa Chaos Basin, California. *Geological Society of America Bulletin*, *105*(9), 1190–1213. https://doi.org/10.1130/0016-7606(1993)105<1190:PROTDV>2.3.CO;2

Workman, J. B., Menges, C. M., Page, W. R., Ekren, E. B., Rowley, P. D., & Dixon, G. L. (2002). Tectonic map of the Death Valley ground-water model area, Nevada and California. In *Miscellaneous Field Studies Map—U. S. Geological Survey* (pp. 58, 1 sheet). U. S. Geological Survey. http://search.proquest.com/georef/docview/2362187962/F4FE00D2FEEF4A9DPQ/2

Wright, L. A. (Lauren A., & Troxel, B. W. (Bennie W. (1968). *Talc deposits of the Southern Death Valley-Kingston Range region, California*. [Sacramento] : Division of Mines and Geology. http://archive.org/details/talcdepositsofso95wrig

Wright, L. A., Troxel, B. W., Williams, E. G., Roberts, M. T., & Diehl, P. E. (1976). *Precambrian sedimentary environments of the Death Valley region, eastern California*. Death Valley Publ. Co.; Shoshone; CA. http://0-search.proquest.com.lib.utep.edu/georef/docview/52351472/2DAD0567B15240FFPQ/2?accountid=7121